# Evidence of non-Maxwellian ion velocity distributions in spherical shock-driven implosions

O. M. Mannion [1] W. T. Taitano,[2] B. D. Appelbe,[3] A. J. Crilly [3] C. J. Forrest,[4] V. Yu. Glebov [4] J. P. Knauer,[4]
P. W. McKenty,[4] Z. L. Mohamed,[4] C. Stoeckl,[4] B. D. Keenan [2] J. P. Chittenden,[3] P. Adrian [5] J. Frenje,[5] N. Kabadi,[5]
M. Gatu Johnson,[5] and S. P. Regan[4]

[1]*Sandia National Laboratories, Albuquerque, New Mexico 87185, USA*
[2]*Los Alamos National Laboratory, Los Alamos, New Mexico 87545, USA*
[3]*Centre for Inertial Fusion Studies, The Blackett Laboratory, Imperial College, London SW72AZ, United Kingdom*
[4]*Laboratory for Laser Energetics, University of Rochester, Rochester, New York 14623, USA*
[5]*Plasma Science and Fusion Center, Massachusetts Institute of Technology, Cambridge, Massachusetts 02139, USA*

The ion velocity distribution functions of thermonuclear plasmas generated by spherical laser direct drive implosions are studied using deuterium-tritium (DT) and deuterium-deuterium (DD) fusion neutron energy spectrum measurements. A hydrodynamic Maxwellian plasma model accurately describes measurements made from lower temperature ($< 10$ keV), hydrodynamiclike plasmas, but is insufficient to describe measurements made from higher temperature more kineticlike plasmas. The high temperature measurements are more consistent with Vlasov-Fokker-Planck (VFP) simulation results which predict the presence of a bimodal plasma ion velocity distribution near peak neutron production. These measurements provide direct experimental evidence of non-Maxwellian ion velocity distributions in spherical shock driven implosions and provide useful data for benchmarking kinetic VFP simulations.

## I. INTRODUCTION

The high energy density (HED) [1] plasmas generated by laser driven inertial confinement fusion (ICF) implosions [2] are used to study basic science relevant to many areas of research including nuclear physics [3], material science [4], and inertial confinement fusion [5]. For these plasmas to be used in controlled scientific studies, the plasma conditions (i.e., temperature, density, and velocity) must be well characterized in each experiment.

Neutron spectroscopy is the most widely used technique to measure the plasma ion temperature when the plasma contains deuterium or a deuterium-tritium (DT) mixture [6–8]. This technique relies on the fact that when plasmas reach sufficiently high ion temperatures ($T_i > 1$ keV) and densities ($\rho \sim 1$ g/cm$^3$), thermonuclear fusion reactions will occur which, in the case of the deuterium-deuterium (DD) and DT reactions, generates neutrons. Calculations have shown [9–12] that the shape of the neutron energy spectrum emitted from a stationary single temperature Maxwellian plasma is a unique function of the plasma ion temperature. In particular, the neutron energy spectrum is normally distributed with a mean given by $\langle E \rangle = E_0 + \Delta E_{th}(T_i)$ and a variance given by $\sigma^2 = \omega_0^2 [1 + \delta_\omega(T_i)]^2 T_i / 5.54$. Here $E_0$ is the zero-temperature fusion product kinetic energy (14.028 MeV for DT and 2.499 MeV for DD), $\Delta E_{th}$ is the Gamow energy shift [13], $\omega_0$ is a constant, and $\delta_\omega$ is a width correction term [10]. The expression for both $\Delta E_{th}$ and $\delta_\omega$ are purely functions of the plasma ion temperature and are given by $\alpha_1 T_i^{2/3}(1 + \alpha_2 T_i^{\alpha_3})^{-1} + \alpha_4 T_i$, where $\alpha_i$ are a set of constants which are defined for $\Delta E_{th}$ and $\delta_\omega$ separately [10].

Neutron energy spectrum measurements are made during ICF experiments using neutron time of flight (nTOF) [6] or magnetic recoil spectrometers [14]. The plasma ion temperature is traditionally inferred by fitting the measured neutron energy spectrum using the single temperature Maxwellian model (i.e., a normal distribution with a mean and variance) [8]. The measured variance is then converted into a plasma ion temperature using the expression described above. For Maxwellian plasmas with temperature gradients in space and time, this fitting procedure gives the mean, or burn averaged, plasma ion temperature of the experiment [12].

In this work it is shown experimentally that the neutron energy spectrum provides unique insights into the plasma ion velocity distribution. Measurements of the first and second moments of the primary DT and DD neutron energy spectrum from plasmas with DT apparent ion temperatures between 3 and 17 keV are presented. A hydrodynamic Maxwellian plasma model accurately describes measurements made from lower temperature ($< 10$ keV) plasmas but is insufficient to describe measurements made from higher temperature plasmas. We use a newly developed theoretical model [15] to show that the neutron energy spectrum measurements from the high temperature plasmas can only be produced by non-Maxwellian ion velocity distributions. These measurements therefore provide direct evidence of a non-Maxwellian ion velocity distribution in these high temperature spherical shock driven implosions.

Furthermore, the high temperature measurements are shown to be more consistent with a bimodal ion velocity distribution than a Maxwellian distribution at peak neutron production using Vlasov-Fokker-Planck (VFP) simulations

TABLE I. Summary of the nominal laser and target initial conditions and the final hot spot conditions achieved for each design. The targets had an initial outer radius of $R_{\text{target}}$, were filled with a DT gas with pressure $P_{\text{fill}}$, and were irradiated with a laser pulse $\Delta t_{\text{laser}}$ in duration with a total energy $E_{\text{laser}}$. The hot spot ion temperature $T_i$ and density $\rho$ are used to estimate the ion mean free path using $\lambda_{ii} \propto T_i^2/\rho$ and equilibration time $\tau_{ii} \propto T_i^{3/2}/\rho$ [16,17]. The final hot spot radius $R_{\text{hs}}$ is used to estimate the plasma Knudsen number using $N_k = \lambda_{ii}/R_{\text{hs}}$ while the nuclear production duration $\tau$ is used to estimate the equilibration time ratio $\tau_N = \tau/\tau_{ii}$ [18].

| Design | $\Delta t_{\text{laser}}$ (ns) | $E_{\text{laser}}$ (kJ) | $R_{\text{target}}$ (μm) | Ablator | $P_{\text{fill}}$ (atm) | $T_i$ (keV) | $\rho$ (g/cm$^3$) | $R_{\text{hs}}$ (μm) | $\tau$ (ps) | $\lambda_{ii}$ (μm) | $N_K$ | $\tau_{ii}$ (ps) | $\tau_N$ |
|---|---|---|---|---|---|---|---|---|---|---|---|---|---|
| A | 1.0 | 26 | 430 | 20 μm CD | 18 | 3 | 1.9 | 40 | 170 | 1 | 0.02 | 2 | 92.1 |
| B | 1.0 | 28 | 560 | 4 μm SiO$_2$ | 10 | 9 | 0.8 | 90 | 120 | 13 | 0.14 | 15 | 8.2 |
| C-R | 0.6 | 12 | 430 | 3 μm SiO$_2$ | 5 | 14 | 0.1 | 90 | 120 | 148 | 1.65 | 141 | 0.9 |
| C | 0.6 | 16 | 420 | 3 μm SiO$_2$ | 5 | 17 | 0.1 | 110 | 120 | 379 | 3.57 | 330 | 0.4 |

and 0-D modeling. This bimodal ion velocity distribution is shown to originate from diffusion of the shock front in these higher temperature more kineticlike implosions. Our work provides a new methodology for directly benchmarking the ion velocity distribution functions calculated in VFP simulations. Previous benchmarking of VFP simulations [19,20] has relied on comparisons of bulk quantities, such as the fusion yield or burn weighted ion temperature, which alone do not possess the unique sensitivity to the ion velocity distribution shape that the neutron spectral moments measurements presented in this work contain.

## II. EXPERIMENTAL RESULTS

Thermonuclear DT plasmas were generated by irradiating spherical targets filled with a DT gas with the OMEGA 60 laser [21] in a spherical direct drive configuration. Three experimental designs were used to achieve the large range of plasma ion temperatures used in this work. A summary of the nominal target design, laser pulse, and canonical plasma conditions achieved by these designs are shown in Table I. Minor variations in the laser and target designs were used to generate a variety of plasma conditions.

The primary DT and DD neutron energy spectra were measured using a suite of nTOF detectors fielded along quasiorthogonal lines of sight (LOS) at the OMEGA 60 laser [22,23]. A normally distributed neutron energy spectrum model was forward fit to each of the measured nTOF signals and the mean and variance were recorded [8]. The ion temperature was inferred from the variance measured along each LOS using the expression described above and is referred to as an "apparent" or "spectrum" ion temperature ($T_s$) [18,24]. The Gamow energy shift was inferred from the set of mean energy measurements made along each LOS [25,26].

### A. Ion Temperature

The minimum DD and DT spectrum ion temperature for each experiment are shown in Fig. 1(a). These measurements reveal that the DD and DT spectrum inferred temperature are nearly identical for the low temperature ($T_{s,DT} < 10$ keV) experiments but diverge for the higher temperature more kineticlike experiments. This trend has been observed in previous work [18] which found that the deuterium and tritium ions do not have sufficient time to equilibrate to a common

temperature in these high temperature shock driven implosions. Table I indeed shows that the equilibration time $\tau_{ii}$ is several times the duration of the neutron production time $\tau$ for the higher temperature experiments.
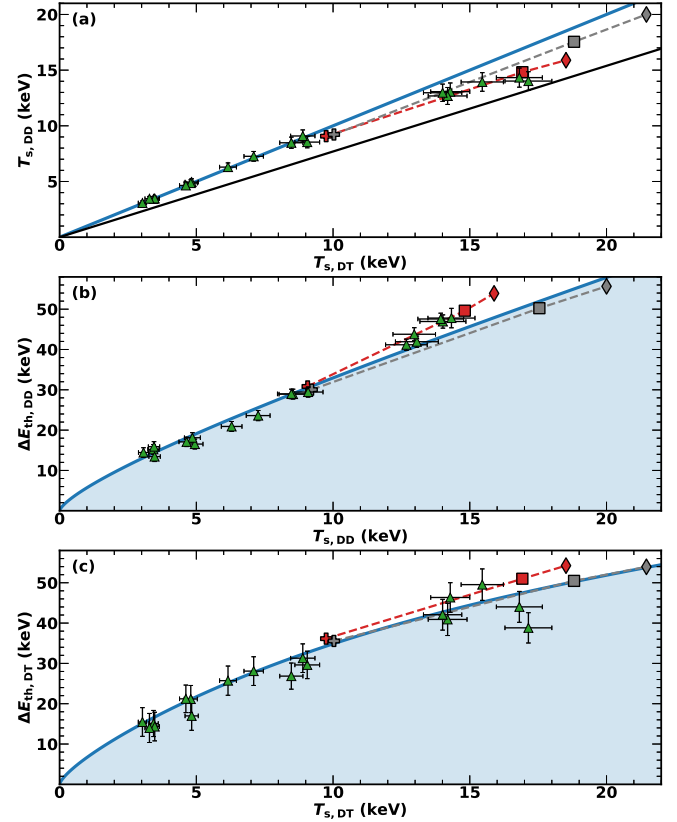


FIG. 1. Summary of the neutron energy spectrum inferred quantities. The experimental data (green triangles), iFP-Kinetic spectrum (red), and iFP-Maxwellian spectrum (gray) results are shown. The iFP results from design B are shown as a cross, design C-R as a square, and design C as a diamond. The expectation for a single temperature 0-D Maxwellian plasma in equilibrium is shown as the solid blue line. The fully thermally decoupled 0-D Maxwellian plasma spectral temperature prediction is shown as the solid black line in (a). The 0-D Maxwellian plasma model serves as an upper bound for the Gamow shift in a Maxwellian plasma, and so the shaded regions in (b) and (c) represent the region accessible by a Maxwellian plasma.

To understand how thermal decoupling of the deuterium and tritium populations can generate the observed trend in Fig. 1(a), we note that the DD spectral temperature can be described as $T_{s,DD}(R) = T_{s,DT}(1 + \alpha)/(1 + \alpha R)$, where $\alpha = m_T/m_D$ and $R = T_T/T_D$ [18,27]. Here $T_D$ and $T_T$ are the deuterium and tritium ion temperatures, respectively. Note this expression does not account for reactivity or spatial profile effects and the plasma is assumed to have a Maxwellian ion velocity distribution function. In the case of a fully equilibrated plasma $R = 1$, and so $T_{s,DD} = T_{s,DT}$. The $T_{s,DD}(R = 1)$ relationship is shown in Fig. 1(a) as the solid blue line and is sufficient to explain the low temperature ($T_{s,DT} < 10$ keV) measurements. In the case when the plasma has been heated by a strong shock and the ions do not have sufficient time to equilibrate, $R = m_T/m_D = 3/2$ [18,28,29]. The $T_{s,DD}(R = 3/2)$ relationship is shown in Fig. 1(a) as the solid black line. We see that the higher temperature plasma experiments indeed approach the fully thermally decoupled limit at the highest of temperatures, indicating that thermal decoupling is a plausible explanation for this observed trend.

Although thermal decoupling appears to explain the ion temperature measurements in Fig. 1(a), and indeed is likely a contributing factor, the ion temperature measurements alone do not uniquely rule out other potential hypotheses which could explain these measurements. For example, residual motion of the plasma can result in $T_{s,DT} > T_{s,DD}$ [30,31] in a way similar to the trend observed in Fig. 1(a). Additionally, as shown in Table I, the ion mean free path in the high temperature experiments is several times the size of the final fusion plasma which suggests that additional kinetic processes could be occurring in the plasma. For example, Knudsen tail depletion [32] is a process by which high energy ions escape the plasma without interacting, resulting in a tail depleted ion velocity distribution function. The inability of the ion temperature alone to rule out residual flow effects or the presence of a non-Maxwellian ion velocity distribution therefore motivates making additional measurements to better constrain the system.

### B. Gamow Shift

Recent theoretical work [15] has shown that measurements of both the Gamow energy shift and the spectrum ion temperature can be used to determine the presence of a non-Maxwellian ion velocity distribution. It was shown that any Maxwellian plasma will result in measured pairs of $(\Delta E_{th,i}, T_{s,i})$ which lay in a region of phase space below that predicted by a 0-D Maxwellian plasma model curve. The 0-D Maxwellian model assumes the plasma is in local thermodynamic equilibrium ($T_D = T_T$), has no residual motion, and has no spatial gradients. When the Maxwellian plasma has spatial gradients or residual fluid motion, the measured pair $(\Delta E_{th,i}, T_{s,i})$ will always reside below the 0-D Maxwellian curve. Therefore, simultaneous measurements of both the Gamow energy shift and spectrum temperature provide a unique measurement to test for the presence of a non-Maxwellian ion velocity distribution in a plasma.

The measured Gamow energy shift is shown as a function of the minimum spectrum ion temperature for the DD

reaction in Fig. 1(b) and the DT reaction in Fig. 1(c). The 0-D Maxwellian plasma model is shown as the solid blue line while the shaded region represents the phase space accessible by a Maxwellian plasma. It should be noted that the shaded region in Fig. 1 simply illustrates the region accessible by a Maxwellian plasma. In ICF implosions the range of ion temperatures and plasma velocities in the fusing plasma are such that measurements will tend to lie in a region just below the 0-D Maxwellian model curve [33].

Figure 1(b) and 1(c) shows that both the DD and DT measurements lie on or just below the 0-D Maxwellian prediction for the low temperature ($T_{s,DT} < 10$ keV) experiments, indicating the measurements are consistent with a Maxwellian plasma. For the high temperature experiments, however, Fig. 1(b) shows that all the DD measurements lie above the 0-D Maxwellian model prediction, indicating the measurements are inconsistent with a Maxwellian plasma. For the high temperature DT measurements, a portion of the DT measurements lie above the 0-D Maxwellian line, indicating a non-Maxwellian plasma, while others fall in the shaded region accessible by a Maxwellian plasma.

The measurements which fall above the 0-D Maxwellian curve therefore provide unambiguous evidence for the presence of a non-Maxwellian ion velocity distribution in these plasmas. The variability observed in the high temperature DT measurements is hypothesized to be due to varying amounts of residual fluid motion being present in different experiments. As mentioned previously, residual plasma motion leads to inflated spectral ion temperature measurements as well as ion temperature asymmetries. The DT spectrum measurement is more sensitive to this effect than the DD measurement. The Gamow energy shift is not sensitive to fluid velocity effects. Therefore, if residual plasma motion results in a larger spectral ion temperature measurement but does not affect the Gamow energy shift, the measured data point will simply translate to the right in Fig. 1(c), moving the measurement farther into the Maxwellian regime. The amount of residual plasma motion depends on a variety of factors including target uniformity, target offset, laser power nonuniformity, and the stalk and glue used to field the target. These factors can change from shot to shot and result in various amounts of plasma motion being present at peak neutron production. The highest temperature DT measurements, which fall below the 0-D Maxwellian curve, showed anomalously high ion temperature asymmetries which is consistent with enhanced residual fluid motion in those plasmas.

### III. VFP SIMULATIONS

The multi-ion Vlasov-Fokker-Planck (VFP) code iFP [34–37] was used to investigate the high temperature experiments which indicated the presence of a non-Maxwellian ion velocity distribution. iFP numerically solves the VFP equations that describe the dynamics of the ion velocity distribution of each ion species using a discrete velocity grid while the electrons are treated as a fluid. The ion velocity distribution functions are calculated assuming a spherically symmetric plasma with a cylindrically symmetric velocity distribution. iFP is capable of modeling various
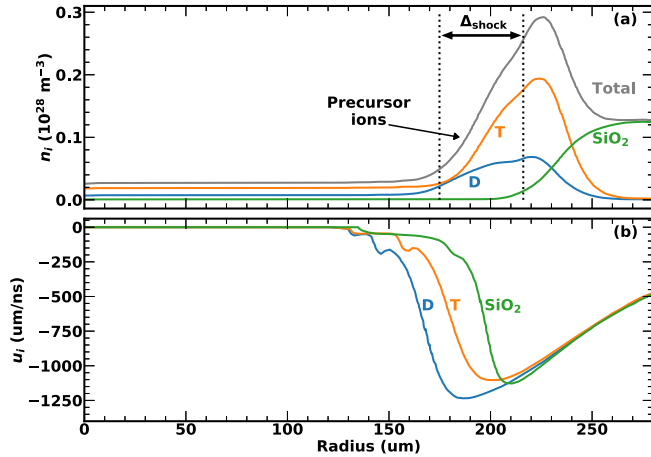
FIG. 2. (a) The ion number density and (b) radial velocity from the iFP simulation of design C when the shell has reached half its initial radius. The triton (orange), deuteron (blue), and SiO$_2$ (green) species are shown in addition to the total number density (gray). The shock width, $\Delta_{shock}$, is shown by the dashed lines and is defined as the distance between the 10% and 90% of the leading edge. The ions in the leading edge of the shock are referred to as precursor ions.

nonhydrodynamic processes [29] such as thermal decoupling (i.e., $T_D \neq T_T$) [18] and ion diffusion [38].

iFP does not have a laser modeling capability and so the one-dimensional radiation hydrodynamic code *LILAC* was used to model the laser energy deposition into the target and the early stages of the implosion. Approximately halfway through the laser pulse, the iFP simulations were initiated using the hydrodynamic profiles from the *LILAC* simulation as initial conditions. The *LILAC* simulation results were used as a boundary condition at the edge of the iFP computational domain.

Simulations were performed for designs B and C. A third simulation was performed using design C, but with a reduced laser power (referred to as design C-R). By lowering the laser power, a weaker shock was generated in this simulation and produced a plasma at intermediate conditions between those generated by designs B and C. These sets of simulations spanned the region of plasma conditions achieved in the experiments where a transition was observed from Maxwellian to non-Maxwellian behavior.

The in-flight ion number density and velocity profiles from the iFP simulation of design C are shown in Fig. 2. The width of the shock front, $\Delta_{shock}$, is $\sim$41 $\mu$m, which is substantially larger than that predicted from a classical hydrodynamic model [$\Delta_{shock}^{hydro} \sim \lambda_{ii} \sim \mathcal{O}(1\ \mu m)$]. This broadening of the shock front has been observed previously [38,39] and is due to high temperature ions permeating ahead of the hydrodynamic shock front due to their increased mobility in the kinetic simulations. We refer to the ions which run ahead of the bulk of the shock front as precursor ions in this work. Furthermore, Fig. 2(b) shows that the concentration of deuterons in the precursor region is larger than the triton concentration. This arises from the fact that deuterons are hotter than the tritons in the precursor region of the shock front [38] and they are less massive than tritons, resulting in the deuteron thermal
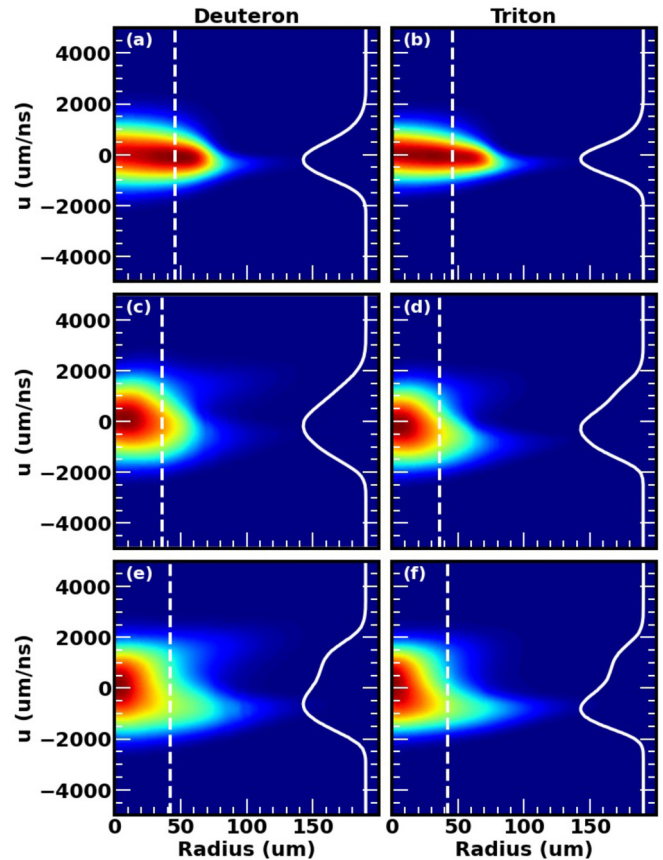


FIG. 3. The iFP deuteron (left column) and triton (right column) ion velocity distributions at peak neutron production for (a), (b) design B; (c), (d) design C-R; (e),(f) design C as a function of the radial velocity and target radius. A lineout of the ion velocity distribution function at the radius of peak neutron production (dashed white line) is shown as a solid white line in each image. The color map and lineouts have been peak normalized for each plot and are both on a linear scale.

velocity ($v_{th} \propto \sqrt{T/m}$) being higher than the triton thermal velocity.

As the implosion proceeds, the precursor ions, which run ahead of the shock front, reach the implosion core much earlier than the ions in the bulk of the shock front. Just prior to peak neutron production, the precursor ions pass through the origin and begin to interact with the still imploding bulk population. Peak neutron production occurs shortly after the bulk ion population begins to converge at the origin, and so there exists a large counterstreaming ion population at peak neutron production. This asynchronous convergence of the shock front results in a highly non-Maxwellian ion velocity distribution being present at peak neutron production and is shown in Figs. 3(e) and 3(f). A lineout of the ion velocity distribution function is also shown in Fig. 3 and highlights the counterstreaming ion population which has a characteristic bimodal structure. The counterstreaming ion population is more pronounced in the case of deuterons [see Figs. 3(e) and 3(f)] due to a larger concentration of deuterons being present in the precursor region of the shock front inflight, which enhances this effect. It should be noted that previous VFP calculations

[19] of shock driven D $^3$He implosions [40] using the code FPION [41,42] have also shown this bimodal ion velocity distribution.

Although similar kinetic modifications of the shock front were also observed in the simulation for design B, the ion velocity distribution at peak neutron production in this simulation was Maxwellian [see Figs. 3(a) and 3(b)]. This is a direct consequence of the lower ion temperature and higher density achieved in design B which results in a shorter ion mean free path as compared to design C (see Table I). The shorter ion mean free path enables the counterstreaming ion population to quickly thermalize with the bulk population in design B and results in a Maxwellian distribution at peak neutron production.

The results from the simulation of design C-R, which achieved a lower plasma ion temperature (and therefore shorter mean free path) as compared to design C, shows an intermediate condition where some thermalization of the counterstreaming population has occurred, but asymmetries still exist in the ion velocity distribution [see Figs. 3(c) and 3(d)].

## IV. KINETIC NEUTRON ENERGY SPECTRUM

To connect these simulation results to the experimental data, the DD and DT neutron energy spectra were calculated for each iFP simulation using the full ion velocity distribution [43]. An additional set of neutron energy spectrum calculations were performed for each iFP simulation where, instead of using the full iFP ion velocity distribution function to calculate the neutron energy spectrum, a Maxwellian approximation (i.e., a Maxwellian with the same mean and variance as the full ion velocity distribution function) was used. By comparing the neutron spectrum calculated using the full ion velocity distribution function (iFP-Kinetic) to those calculated using the Maxwellian approximation of the full ion velocity distribution function (iFP-Maxwellian), the effect that the shape of the ion velocity distribution has on the neutron energy spectrum can be studied while preserving the same bulk properties of the full ion velocity distribution function. The neutron energy spectra calculated from the iFP simulations of designs B and C are shown in Fig. 4.

A fit using the same neutron energy spectrum model that was applied to the experimental data was applied to the iFP spectra to quantify the differences between the first and second moments of the iFP-Kinetic and iFP-Maxwellian neutron spectra. The neutron energy spectrum variances were used to infer the spectrum ion temperature using the same method as was applied to the experimental data, and the Gamow energy shift was inferred from the mean energy of the neutron spectrum. The iFP neutron spectrum values are compared to the experimental data in Fig. 1.

For design B, one expects there to be no difference between the iFP-Maxwellian and iFP-Kinetic neutron spectrum as the iFP ion velocity distribution was found to be Maxwellian (see Fig. 3). Figure 4 shows that indeed, the DD and DT neutron energy spectra are identical between the iFP-Maxwellian and iFP-Kinetic calculation for this design. Additionally, Fig. 1 shows that the Gamow energy shift and spectrum
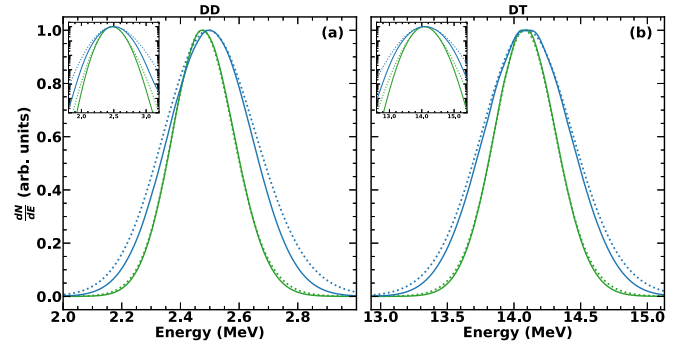


FIG. 4. (a) The DD and (b) DT iFP-Maxwellian (dotted) and iFP-Kinetic (solid) neutron energy spectra for design B (green) and design C (blue). The insets show the same curves but on a log scale. The differences between the iFP-Maxwellian and iFP-Kinetic spectra for design C are a direct consequence of the non-Maxwellian ion velocity distribution present in this simulation (see Fig. 3).

temperature for design B are identical and consistent with the 0-D Maxwellian plasma model as expected.

For designs C and C-R one expects a deviation between the iFP-Maxwellian and iFP-Kinetic neutron spectrum based on the non-Maxwellian ion velocity distribution observed in these simulations (see Fig. 3). Figure 4 shows that the iFP-Kinetic neutron energy spectra for design C are narrower than the iFP-Maxwellian spectra while the mean energy appears to be unchanged between the two spectra. As a result, the spectrum inferred ion temperature from the iFP-kinetic spectra are less than that from the iFP-Maxwellian spectra. This can be seen in Fig. 1 which shows that the iFP-Kinetic spectrum temperature is lower for the iFP-Maxwellian results. Furthermore, we see in Figs. 1(b) and 1(c) that the Gamow energy shift appears unchanged between the two calculations, but the spectrum temperatures are different. Consequentially, the Gamow energy shift inferred from the iFP-Kinetic spectra for designs C and C-R fall outside of the region accessible by a Maxwellian plasma.

By comparing the iFP-Maxwellian and iFP-Kinetic results we can distinguish the effects of the non-Maxwellian ion velocity distribution on the neutron inferred values. In particular, the iFP-Maxwellian spectral temperature measurements in Fig. 1 show that a portion of the discrepancy between the DD and DT values is indeed due to thermal decoupling. The remaining discrepancy is only explained by the iFP-Kinetic values, which account for the non-Maxwellian ion velocity distribution effects.

When comparing the totality of measurements presented in Fig. 1 it is clear the iFP-Kinetic spectrum explains the measurements and a Maxwellian model is insufficient. Specifically, the high temperature iFP-Kinetic Gamow shift and spectral temperature measurements fall outside of the region accessible by a Maxwellian plasma which is also observed experimentally.

## V. CONCLUSIONS

In summary, measurements of the DT and DD neutron energy spectrum emitted from DT plasmas generated by laser driven implosions were used to study the plasma ion

velocity distribution. Measurements from lower temperature, more hydrodynamiclike plasmas were found to agree with a Maxwellian model, while measurements from higher temperature, more kineticlike plasmas did not. The neutron energy spectrum calculated from Vlasov-Fokker-Planck simulations were found to agree with the high temperature DD measurements, while some discrepancies, hypothesized to be due to residual kinetic energy in the plasma, existed for the DT measurements. These VFP simulations revealed that ion kinetic effects near the shock front leads to an asynchronous shock convergence that results in a bimodal ion velocity distribution being present at peak neutron production in the high temperature experiments.

This work builds upon previous experimental [18,40,44,45] and simulation studies [19,20] of shock driven implosions. In particular we have used a unique property of the detailed shape of the neutron energy spectrum to provide evidence of a non-Maxwellian ion velocity distribution in our experiments. Previous work has relied on measurements of bulk quantities such as the fusion yield and spectral ion temperature which alone cannot uniquely identify the presence of non-Maxwellian ion velocity distributions as these measurements are sensitive to other physical processes potentially occurring in the experiment. By simultaneously measuring the spectral ion temperature and the Gamow energy shift, we provide unambiguous evidence for a non-Maxwellian ion velocity distribution in our experiments and provide a data set which can be used to benchmark future VFP calculations. Furthermore, the VFP simulations presented in this work were used to calculate the full shape of the neutron energy spectrum from the ion velocity distribution. This improves upon previous work which calculated spectral ion temperatures from VFP simulations using a mass weighted temperature, which will be unaffected by the subtleties of the full neutron spectrum shape.

Finally, measurements of the spectrum ion temperature and Gamow energy shift from burning plasma experiments at the National Ignition Facility (NIF) have observed similar trends as shown in Figs. 1(b) and 1(c) [33]. The NIF measurements indicate the presence of a non-Maxwellian ion velocity distribution in the burning plasmas, the source of which is not well understood. The detailed understanding developed in this work can help provide insights into the physical mechanisms effecting these burning plasmas.

[1] R. P. Drake, Phys. Plasmas **16**, 055501 (2009).

[2] J. Nuckolls, L. Wood, A. Thiessen, and G. Zimmerman, Nature (London) **239**, 139 (1972).

[3] D. T. Casey *et al.*, Nat. Phys. **13**, 1227 (2017).

[4] T. Döppner D. C. Swift, A. L. Kritcher, B. Bachmann, G. W. Collins, D. A. Chapman, J. Hawreliak, D. Kraus, J. Nilsen, S. Rothman, L. X. Benedict, E. Dewald, D. E. Fratanduono, J. A. Gaffney, S. H. Glenzer, S. Hamel, O. L. Landen, H. J. Lee, S. LePape, T. Ma, M. J. MacDonald, A. G. MacPhee, D. Milathianaki, M. Millot, P. Neumayer, P. A. Sterne, R. Tommasini, and R. W. Falcone, Phys. Rev. Lett. **121**, 025001 (2018).

[5] J. A. Frenje, P. E. Grabowski, C. K. Li, F. H. Seguin, A. B. Zylstra, M. Gatu Johnson, R. D. Petrasso, V. Y. Glebov, and T. C. Sangster, Phys. Rev. Lett. **115**, 205001 (2015).

[6] R. A. Lerche, L. W. Coleman, J. W. Houghton, D. R. Speck, and E. K. Storm, Appl. Phys. Lett. **31**, 645 (1977).

[7] M. Tardocchi, G. Gorini, H. Henriksson, and J. Källne, Rev. Sci. Instrum. **75**, 661 (2004).

[8] R. Hatarik *et al.*, J. Appl. Phys. **118**, 184502 (2015).

[9] H. Brysk, Plasma Phys. **15**, 611 (1973).

[10] L. Ballabio, J. Källne, and G. Gorini, Nucl. Fusion **38**, 1723 (1998).

[11] B. Appelbe and J. Chittenden, Plasma Phys. Controlled Fusion **53**, 045002 (2011).

[12] D. H. Munro, Nucl. Fusion **56**, 036001 (2016).

[13] $\Delta E_{\text{th}} = \gamma \langle K \rangle + \beta \langle V^2 \rangle$, where $\gamma$ and $\beta$ are constants, $K$ and $V$ are the relative kinetic energy and center of mass velocity of the reactant ions, respectivly. The average $\langle \rangle$ is taken over the ion velocity distribution weighted by the fusion cross section. See Ref. [10] for details.

[14] J. A. Frenje *et al.*, Rev. Sci. Instrum. **79**, 10E502 (2008).

[15] A. J. Crilly, B. D. Appelbe, O. M. Mannion, W. Taitano, E. P. Hartouni, A. S. Moore, M. Gatu-Johnson, and J. P. Chittenden, Nucl. Fusion **62**, 126015 (2022).

[16] A. S. Richardson *et al.*, *2019 NRL Plasma Formulary* (Naval Research Laboratory, 2019), https://books.google.com/books/about/2019_NRL_Plasma_Formulary.html?id=UkRCzwEACAAJ.

[17] $\rho = (\rho R)_{\text{hs}}/R_{\text{hs}}$ for design B and C where $(\rho R)_{\text{hs}}$ and $R_{\text{hs}}$ are the measured hot spot areal density and radius respectively. $\rho =$

$\rho_i (R_{\text{target}}/R_{\text{hs}})^3$ for design A as the hot spot areal density was not measured. $\rho_i$ is the initial gas mass density.

[18] N. V. Kabadi, R. Simpson, P. J. Adrian, A. Bose, J. A. Frenje, M. GatuJohnson, B. Lahmann, C. K. Li, C. E. Parker, F. H. Seguin, G. D. Sutcliffe, R. D. Petrasso, S. Atzeni, J. Eriksson, C. Forrest, S. Fess, V. Y. Glebov, R. Janezic, O. M. Mannion, H. G. Rinderknecht, M. J. Rosenberg, C. Stoeckl, G. Kagan, M. Hoppe, R. Luo, M. Schoff, C. Shuldberg, H. W. Sio, J. Sanchez, L. B. Hopkins, D. Schlossberg, K. Hahn, and C. Yeamans, Phys. Rev. E **104**, L013201 (2021).

[19] O. Larroche, H. G. Rinderknecht, M. J. Rosenberg, N. M. Hoffman, S. Atzeni, R. D. Petrasso, P. A. Amendt, and F. H. Séguin, Phys. Plasmas **23**, 012701 (2016).

[20] O. Larroche, H. G. Rinderknecht, and M. J. Rosenberg, Phys. Rev. E **98**, 031201(R) (2018).

[21] T. R. Boehly et al., Opt. Commun. **133**, 495 (1997).

[22] C. J. Forrest, V. Y. Glebov, V. N. Goncharov, J. P. Knauer, P. B. Radha, S. P. Regan, M. H. Romanofsky, T. C. Sangster, M. J. Shoup, III, and C. Stoeckl, Rev. Sci. Instrum. **87**, 11D814 (2016).

[23] O. M. Mannion, J. P. Knauer, V. Y. Glebov, C. J. Forrest, A. Liu, Z. L. Mohamed, M. H. Romanofsky, T. C. Sangster, C. Stoeckl, and S. P. Regan, Nucl. Instrum. Methods Phys. Res., Sect. A **964**, 163774 (2020).

[24] M. Gatu Johnson et al., Rev. Sci. Instrum. **89**, 10I129 (2018).

[25] R. Hatarik, R. C. Nora, B. K. Spears, M. J. Eckart, G. P. Grim, E. P. Hartouni, A. S. Moore, and D. J. Schlossberg, Rev. Sci. Instrum. **89**, 10I138 (2018).

[26] O. M. Mannion et al., Rev. Sci. Instrum. **92**, 033529 (2021).

[27] A. Inglebert, B. Canaud, and O. Larroche, Europhys. Lett. **107**, 65003 (2014).

[28] This relationship is derived assuming a strong shock has heated the plasma such that the ion temperature of each species in the plasma is given by $T_{i,j} \propto m_j/(1 + Z_j)$ [29].

[29] B. D. Keenan, A. N. Simakov, W. T. Taitano, and L. Chacón, Phys. Plasmas **25**, 032103 (2018).

[30] T. J. Murphy, Phys. Plasmas **21**, 072701 (2014).

[31] K. M. Woo et al., Phys. Plasmas **25**, 102710 (2018).

[32] K. Molvig, N. M. Hoffman, B. J. Albright, E. M. Nelson, and R. B. Webster, Phys. Rev. Lett. **109**, 095001 (2012).

[33] E. P. Hartouni et al., Nat. Phys. **19**, 72 (2023).

[34] W. T. Taitano, L. Chacón, A. N. Simakov, and K. Molvig, J. Comput. Phys. **297**, 357 (2015).

[35] W. T. Taitano, L. Chacón, and A. N. Simakov, J. Comput. Phys. **318**, 391 (2016).

[36] W. T. Taitano, L. Chacón, and A. N. Simakov, J. Comput. Phys. **339**, 453 (2017).

[37] W. T. Taitano, A. N. Simakov, L. Chacón, and B. Keenan, Phys. Plasmas **25**, 056310 (2018).

[38] B. D. Keenan, A. N. Simakov, L. Chacon, and W. T. Taitano, Phys. Rev. E **96**, 053203 (2017).

[39] S. E. Anderson, L. Chacon, W. T. Taitano, A. N. Simakov, and B. D. Keenan, Phys. Rev. E **104**, 055205 (2021).

[40] M. J. Rosenberg, H. G. Rinderknecht, N. M. Hoffman, P. A. Amendt, S. Atzeni, A. B. Zylstra, C. K. Li, F. H. Seguin, H. Sio, M. G. Johnson, J. A. Frenje, R. D. Petrasso, V. Y. Glebov, C. Stoeckl, W. Seka, F. J. Marshall, J. A. Delettrez, T. C. Sangster, R. Betti, V. N. Goncharov, D. D. Meyerhofer, S. Skupsky, C. Bellei, J. Pino, S. C. Wilks, G. Kagan, K. Molvig, and A. Nikroo, Phys. Rev. Lett. **112**, 185001 (2014).

[41] O. Larroche, Phys. Fluids B **5**, 2816 (1993).

[42] O. Larroche, Eur. Phys. J. D **27**, 131 (2003).

[43] B. D. Appelbe, W. T. Taitano, A. J. Crilly, O. M. Mannion, C. J. Forrest, and J. P. Chittenden, arXiv:2305.02403.

[44] M. J. Rosenberg et al., Phys. Plasmas **22**, 062702 (2015).

[45] H. G. Rinderknecht, H. Sio, C. K. Li, A. B. Zylstra, M. J. Rosenberg, P. Amendt, J. Delettrez, C. Bellei, J. A. Frenje, M. G. Johnson, F. H. Séguin, R. D. Petrasso, R. Betti, V. Y. Glebov, D. D. Meyerhofer, T. C. Sangster, C. Stoeckl, O. Landen, V. A. Smalyuk, S. Wilks, A. Greenwood, and A. Nikroo, Phys. Rev. Lett. **112**, 135001 (2014).